

Particles II

Access the latest eBook →

11

Advanced
Optical Metrology

Particles II



EVIDENT
OLYMPUS

WILEY

Impact on Biological Systems and the Environment

This eBook is dedicated to the research of Professor David Wertheim.

In collaboration with various groups, Professor Wertheim uses confocal microscopy to analyse the impact of different types of particles on human health and the environment, with a focus on human health-hazardous particles detected with solid-state nuclear track detectors (SSNTD). Download for free, today.

EVIDENT
OLYMPUS

WILEY

Perovskite Plasticity: Exploiting Instability for Self-Optimized Performance

Julia S. van der Burgt, Francesca Scalerandi, Jeroen J. de Boer, Susan A. Rigter, and Erik C. Garnett*

Halide perovskites display outstanding photoluminescence quantum yield, tunable emission, and simple deposition, which make them attractive for optoelectronics. At the same time, their facile ion migration and transformation under optical, electrical, and chemical stress are seen as a major limitation. Mixed halide perovskites are particularly problematic since optical excitation can cause changes in the bandgap that are detrimental for solar cell and light-emitting diode efficiency and stability. In this work, instead of preventing such changes, photo-induced halide segregation in perovskites is exploited to enable responsive, reconfigurable, and self-optimizing materials. The mixed halide perovskite film is trained to give directional light emission using a nanophotonic microlens; through a self-optimized process of halide photosegregation, the system mimics the training stimulus. Longer training leads to more highly directional emission, while different halide migration kinetics in the light (fast training) and dark (slow forgetting) allows for material memory. This self-optimized material performs significantly better than lithographically aligned quantum dots because it eliminates lens-emitter misalignment and automatically corrects for lens aberrations. The system shows a combination of mimicking, improving over time, and memory, which comprise the basic requirements for learning, and allow for the intriguing prospect of intelligent optoelectronic materials.

their dynamic nature has been seen as a major limitation to implementing them in applications that require long-term stability,^[6–9] such as solar cells and light emitting diodes.^[10–14] In contrast, the push toward intelligent materials has largely taken inspiration from natural and living systems, where instability (material turnover and regeneration) is essential for environmental adaptation, optimized properties, and learning.^[15,16] By altering the response and regeneration timescale, nature can span from slowly optimizing and relatively stable materials to those that are much less stable but also respond more quickly. There are now synthetic analogues trying to span this continuum as well. For example, the ability of bone to strengthen itself in response to mechanical forces has been artificially mimicked with composite materials that cross-link upon mechanical loading.^[17] Neuromorphic computing lies on a faster time scale,^[18] where self-learning optical neurosynaptic networks are being pursued to mimic brain plasticity, due to the broad bandwidth and high speed inherent to optical systems.^[19]

The combination of rapid ion migration, sensitivity to many external stimuli, and outstanding optoelectronic properties displayed by halide perovskites makes them the ideal platform for the next generation of reconfigurable, responsive, programmable, and intelligent materials.^[20] In this work, we exploit a photoinstability (light-induced halide segregation) to train a mixed halide perovskite thin film to display user-defined optical properties. Our case study consists of a mixed halide perovskite thin film that is trained to give highly directional light emission using a nanophotonic microlens and exploiting the rules of reciprocity. It exhibits many of the most attractive behaviors being sought out for responsive, adaptive, intelligent, and self-learning materials. First, it interacts with its environment by receiving a certain input (highly collimated light excitation) and adapting its structure to transform initially isotropic emission into highly directional emission, effectively mimicking the training input. In addition to this responsive behavior, it remembers over time: the longer the system is trained with the excitation input, the better the performance, and consecutive light/dark cycles show faster retraining, slower forgetting, and better final performance. The system self-optimizes

1. Introduction

Halide perovskites have found many potential applications in the field of optoelectronics due to their outstanding photoluminescence quantum yield, tunable emission wavelength and simple solution or vapor-phase deposition.^[1–5] However, the instability of halide perovskites that results from

J. S. van der Burgt, F. Scalerandi, J. J. de Boer, S. A. Rigter, E. C. Garnett
AMOLF Institute
Science Park 104, 1098XG Amsterdam, Netherlands

S. A. Rigter, E. C. Garnett
Institute of Physics
University of Amsterdam
Science Park 904, 1098XH Amsterdam, Netherlands
E-mail: e.c.garnett@uva.nl

 The ORCID identification number(s) for the author(s) of this article can be found under <https://doi.org/10.1002/adfm.202203771>.

© 2022 The Authors. Advanced Functional Materials published by Wiley-VCH GmbH. This is an open access article under the terms of the Creative Commons Attribution License, which permits use, distribution and reproduction in any medium, provided the original work is properly cited.

DOI: 10.1002/adfm.202203771

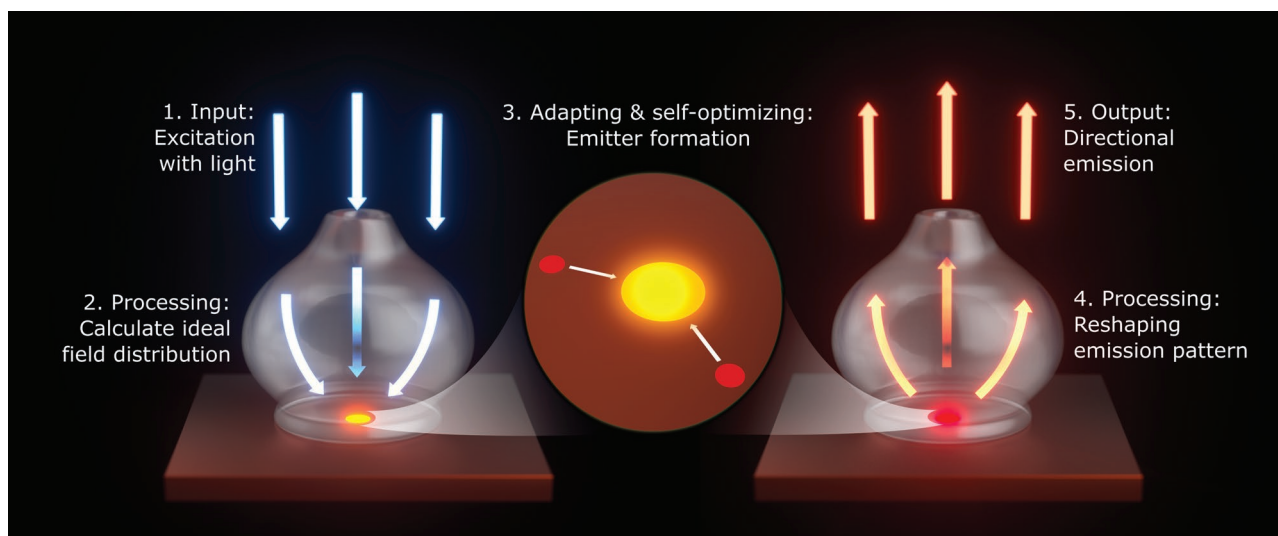


Figure 1. Training perovskite for highly directional light emission. A dielectric microlens of $\approx 7 \mu\text{m}$ in size is placed on top of a methylammonium lead iodide/bromide perovskite film ($\text{MAPb}(\text{I}_{0.5}\text{Br}_{0.5})_3$). When excited by plane wave illumination (step 1), the microlens reshapes the electric field into a strong hotspot (step 2). This causes photosegregation of the halides in the mixed halide perovskite, through which the perovskite adapts and self-optimizes to form an iodide-rich region in the hotspot (step 3). This lower bandgap region acts as a localized emitter. The emitted light is again processed by the lens (step 4) into the desired output of highly directional emission (step 5).

and is therefore robust against fabrication imperfections, and converges to a global optimum without getting stuck in a local optimum. The self-optimization results in performance significantly beyond what can be achieved by design and nanolithography. This shows that by harvesting the right dynamics, we can transform the instability of mixed halide perovskites from a bug into a feature.

2. Results

The system, consisting of nanophotonic microlenses on top of a perovskite film, is depicted schematically in **Figure 1**. It consists of a dielectric microlens ($\approx 7 \mu\text{m}$ in size) on top of a film of methylammonium lead iodide/bromide perovskite ($\text{MAPb}(\text{I}_{0.5}\text{Br}_{0.5})_3$). Upon exposure to light, this material shows phase segregation leading to iodide-rich regions with a lower bandgap energy. Due to exciton funneling toward these regions, photosegregation results in strong and localized emission from the iodide-rich regions,^[21] while surrounding areas with increased bromide content will not contribute to emission.^[22] The exact mechanism of this phase segregation and the resulting local compositions are still under debate^[23–26] and not the focus of this study. With the microlens, we are able to control the photosegregation and the resulting localized emission, to obtain a desired light output. The process is indicated schematically in **Figure 1** and can be described as follows. Upon light exposure (step 1), the microlens processes the incoming signal to a reshaped electric field distribution underneath the lens (step 2). In this case, we shape the field to a single hotspot of strong field enhancement. Under influence of the optical field, the mixed halide perovskite adapts and optimizes itself through photosegregation in the hotspot (step 3). A small iodide-rich region is formed, which acts as a localized emitter.

The photoluminescence emitted from this region is again processed by the lens (step 4) into the desired pattern of highly directional emission (step 5).

Before studying the full system, the properties of the spin-coated $\text{MAPb}(\text{I}_{0.5}\text{Br}_{0.5})_3$ film without lenses are studied. Characterization of the film confirmed successful formation of perovskite (**Figure S1**, Supporting Information) with a bandgap of 1.9 eV (**Figure S2**, Supporting Information) and small grains, which lead to stronger photosegregation.^[23,27] The grains are made sufficiently smaller than the lenses, such that the substrate is effectively homogeneous and lenses will always be positioned on grain boundaries. Time resolved emission spectra in **Figure 2a** show the expected vanishing of the initial peak at 660 nm, corresponding to fully mixed $\text{MAPb}(\text{I}_{0.5}\text{Br}_{0.5})_3$, and the appearance of a peak starting at 700 nm and red-shifting further to stabilize at 740 nm. This is the expected emission of the segregated $\text{MAPb}(\text{I}_{0.8}\text{Br}_{0.2})_3$, the phase in which any mixed iodide/bromide perovskite with bromide content above 0.2 is known to segregate.^[13,28]

Measurements of repeated cycles of light exposure alternating with a one-minute recovery in the dark reveal that this material can be trained and has memory; consecutive cycles show faster and stronger phase segregation, as visible in **Figure 2b**. Although in the dark, the perovskite returns to its mixed state, some atomic-scale changes remain, which allow the next cycle of phase segregation to happen faster.^[29] We speculate that either a small nucleus of the low bandgap phase remains, which avoids the nucleation barrier in subsequent light exposures, or that the grain structure is modified such that the ionic diffusion is faster. Experiments to differentiate between these possible mechanisms are ongoing and will not be discussed here. Extending the dark time revealed that it takes up to 1 h for the material to fully return to its original state (**Figure S3**, Supporting Information). This combination of

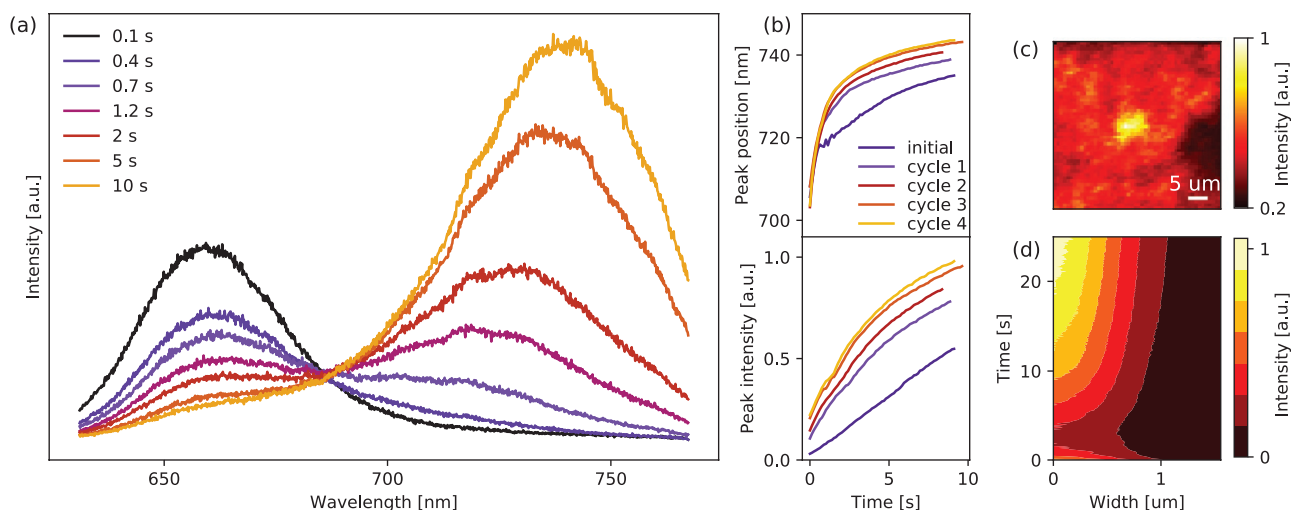


Figure 2. Phase segregation dynamics in the MAPb(I_{0.5}Br_{0.5})₃ film under 405 nm focused laser excitation. a) Emission spectra at increasing exposure times. The peak at 660 nm, corresponding to the mixed phase, disappears and a new peak at longer wavelength appears and grows over time, corresponding to the formation of an iodide-rich region. b) Development of peak position and intensity over several excitation cycles, alternating with a 1-min recovery in the dark. After the first illumination, the material responds faster. c) Spatial map of the emission intensity between 740 and 760 nm around a previously illuminated spot. A local emitter is formed. d) Emitter spot size over time, obtained from real space image as the average radial intensity. The emission is first quenched upon nucleation of the emitter, and then increases while the emitter grows.

fast dynamics in the light with slow recovery in the dark, allows for dynamically reconfigurable short term memory. The localized emission spot from a region that was previously excited with a high intensity shown in Figure 2c confirms this memory effect and the light-induced local emitter formation.

The time dynamics of the emitter formation are investigated with real-space images of the film under focused laser excitation. Figure 2d shows the spot size as a function of time, obtained by taking the average radial intensity. First, a rapid decrease in emitter spot size is observed, followed by an increase and gradual saturation. The initial decrease is in agreement with the spectral response in Figure 2a, where the initial peak at 660 nm disappears before the second peak starts to appear. This indicates that the emission is quenched upon the initial nucleation of the segregated region. When the light is off, some of this nucleation or other atomic scale changes remain; in the next cycle, photosegregation occurs faster and the emitter is immediately formed (Figure S4, Supporting Information).

To further support our claim of locally forming an iodide-rich region, we have investigated the nature of the photobrightening in the process. Besides photosegregation, photobrightening has also previously been observed through photochemical surface passivation via environmental gasses.^[30] To rule out this surface passivation effect, we encapsulate our samples with aluminum oxide to enhance stability and shield them from the environment.^[31] We compared samples of pure bromide perovskite with and without encapsulation. Without encapsulation, it shows a strong increase in emission intensity upon light soaking, while with encapsulation, photodarkening occurs (Figure S5, Supporting Information),^[32] indicating that the encapsulation fully blocks the photobrightening. The emission enhancement in our encapsulated mixed halide film (Figure 2a) and the formation of localized emitters can therefore be attributed to halide segregation.

To control the observed photosegregation, we use a nanophotonic structure that reshapes the incoming light field in a designed manner. The self-optimization of our lens-perovskite system relies on the principle of reciprocity, which states that source and detector are interchangeable in an optical system. In our system, light at normal incidence is focused to the location of the hotspot via the microlens, and thus emission from the hotspot also is collimated into a narrow beam in the normal direction. The microlenses used in this study were reported to provide highly directional emission.^[33] The size of these lenses can be optimized to obtain maximal directivity at a desired emission wavelength, which in this case is the wavelength of the iodide-rich regions. This lens design is particularly suitable because it is optimized based on the same principle of reciprocity that we use here for self-alignment.^[34] Simulations predict a total directivity of 46 and a partial directivity within the numerical aperture (NA) of the objective of 38 for this system (Figure S8, Supporting Information), where directivity is defined as the emission power in the desired direction normalized to the average emission power in all directions.^[35]

The directivity measurements were done using a Fourier microscope as described before.^[33] This setup has an objective with a relatively low NA of 0.42, which allows for sufficiently intense excitation with a small spot size, while limiting angular spread in the excitation beam to mimic a spatially confined plane-wave source. Figure 3a shows the typical dynamics of the emission intensity and directivity as a function of time, when a lens is illuminated for the first time. Initially, the intensity rapidly decreases, with a simultaneous increase in directivity. We attribute this behavior to the nucleation of the emitter, in agreement with what we observed when exciting the bare film with a focused laser beam (Figure 2a,d): the emission is first quenched before a red-shifted, enhanced photoluminescence peak rises. The concurrent rapid increase in directivity indicates that the emitter in the hotspot is already forming, and

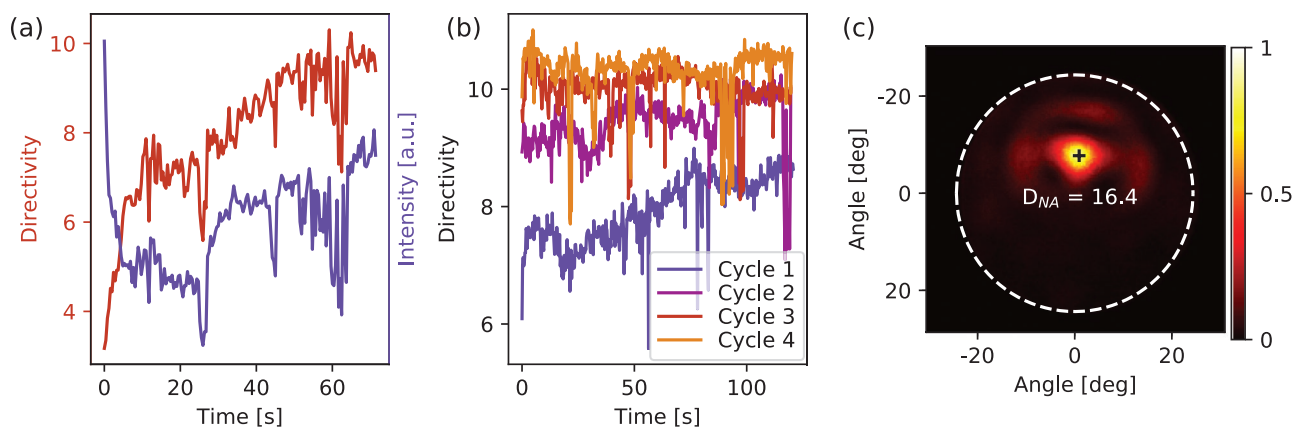


Figure 3. Directivity measurements during training of the lens. a) Directivity and intensity as a function of time upon initial illumination of the lens with a focused 405 nm laser. The directivity increases first rapidly and then more gradually, while the intensity first drops and then gradually increases, due to initial quenching while the emitter nucleates, followed by a growth of the emitter. b) Upon consecutive illumination cycles, alternating with a 1-minute recovery in the dark, the directivity increases each cycle due to training of the perovskite. c) Measured Fourier image of the record directivity that was reached after several cycles of light and dark. The white dashed circle corresponds to the NA of the objective of 0.42.

although the total intensity is low, this emission originates from the hotspot. After the first 10 s, the dynamics slow down. The directivity keeps gradually increasing, and the intensity stabilizes and then starts to increase ≈ 28 s, indicating a growth in emitter strength. Figure 3b shows the effect of several cycles of illumination separated by a 1-min recovery in the dark. Remarkably, the second cycle starts at higher directivity than the end of the first cycle, indicating the system has been trained. Initially, there likely is a competition for iodide between different spots underneath the lens. There are mechanisms through which iodide rich regions can form away from the ideal location: either, another region also receives a small part of the excitation light due to lens imperfections, or inhomogeneities in the multicrystalline perovskite film promote the halide segregation to take place locally, for example at grain boundaries.^[23,27] This initially causes a competition for iodide between these rivaling regions and the designed hotspot, but with continuous training we observe that the designed hotspot prevails. In the dark the halides remix, but the nucleation of the iodide-rich region in the designed hotspot remains, as it is the most well-trained by the excitation light. Upon the next excitation, this region responds faster, as we have seen before, thus having an advantage over other regions that are not designed to be trained. This training behavior and retention results in higher directivity in consecutive cycles, until the system has reached its optimal configuration and the directivity stabilizes in cycles three and four in Figure 3b. The Fourier image of the highest measured directivity of 16.4 is shown in Figure 3c, which was obtained after several cycles of light and dark (Figure S6, Supporting Information).

The proposed mechanism of rivaling iodide-rich regions and subsequent victory of the designed emitter hotspot is confirmed by analyzing the Fourier patterns resulting from prolonged illumination of the system, as shown in Figure 4. On the left, it shows again the directivity and the intensity as a function of time, but now during continuous training (illumination) over the course of half an hour. Initially, the directivity is very low, due to several bright spots in the Fourier image, most of which do not emit into the target angle (panel 1). Although different

spots in Fourier space in general do not necessarily correspond to different real-space emission locations, the presence of the microlens provides a strong correlation between emitter position and angle (Figures S9 and S10, Supporting Information). In Figure 4 the spot closest to the center of the Fourier space images, i.e. normal direction, starts to gain in intensity until point 2. Through competition for iodide, it loses power again, and directivity decreases while intensity remains constant until point 3. Here the system starts to recover and attract more iodide toward the designed hotspot, leading to an increase in intensity and directivity (point 4), until it reaches a maximum directivity of 13.9 in point 5. Then the intensity and directivity suddenly drop (point 6), which can be attributed to damage inflicted to the perovskite during extended exposure to high laser power. Under continuous illumination, it takes the system >15 min to reach the maximum directivity, which is longer than it took during cycles of illumination and dark. This indicates that the emitter has a larger difficulty winning the competition for iodide under prolonged illumination. The emitter in the hotspot, which is trained, has an advantage over rivaling I-rich regions in the competition for iodide, as long as we make use of its retention. While the rivaling spots are “forgotten” during the remixing, the trained spot is retained. The remixing in the dark in combination with the training of the hotspot helps the designed emitter to win the competition for iodide, and thus convergence to the optimal configuration. This behavior shows a remarkable parallel to classical nucleation and growth theory. For example, with the method of melt-recrystallization, large and high quality crystals can be formed by cycling through heating and cooling, where in each cycle the initially nucleated crystal grows. Although the system can lose all memory after an extended period in the dark, the training rate is much faster than the forgetting rate, which allows for dynamically reconfigurable short term memory. Thanks to the self-optimizing processes, a well-trained system performs better than what could be achieved in our previous work, where we used nanolithography to spatially confine and align emitters with lenses.^[33] Fabrication and alignment errors limited the directivity to 12.9, while the self-optimized system results in directivity as high as 16.4.

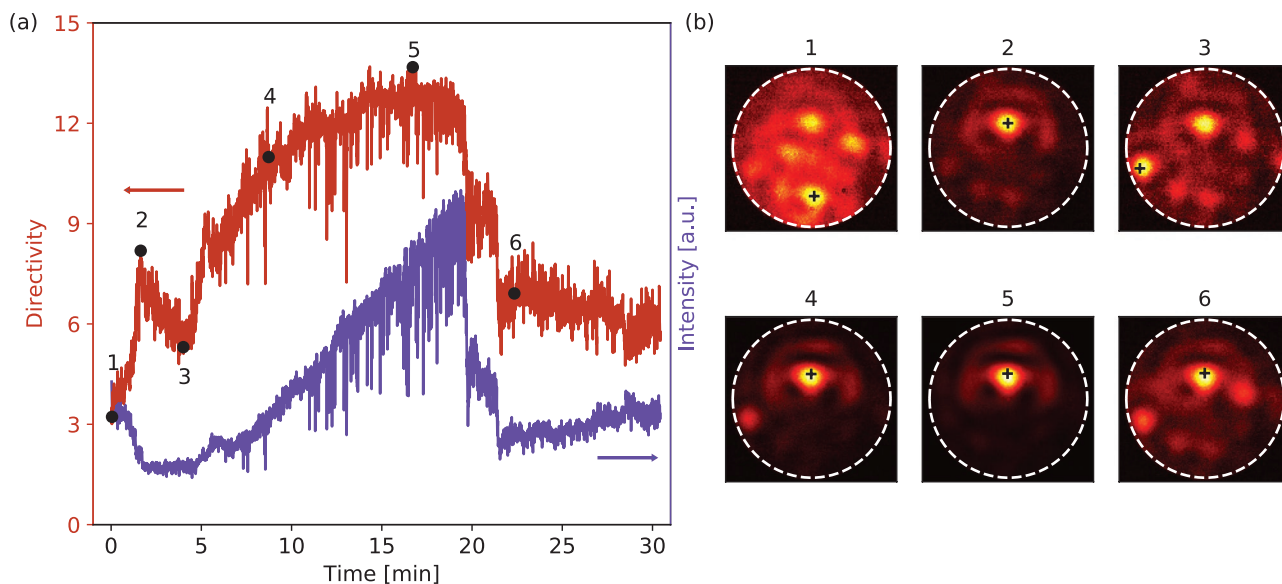


Figure 4. Analysis of the competition for iodide through prolonged illumination. a) Directivity and intensity as a function of time during 30 min of illumination. Under continuous illumination it takes longer to reach the maximum directivity compared to cycles of illumination and dark. b) Fourier images of the points indicated in panel a. Different spots correspond to different emitting regions underneath the lens. A shift in intensity between these spots indicates a change in iodide distribution. The colormaps correspond to different intensity scales, because of the large range of intensities covered. The white dashed circle corresponds to the NA of the objective of 0.42.

3. Conclusions and Outlook

We have demonstrated how we can train a system of mixed halide perovskite with a microlens to self-optimize and retain the optimized configuration for highly directional emission. To do this, we make use of the dynamic nature of the material and the rules of reciprocity. Usually, the dynamic nature of mixed halide perovskites are regarded as unfavorable instability, but this case study shows how we utilize the process of photosegregation to make a system that mitigates fabrication errors in shape and alignment of the microlens, and therefore performs better than its traditional counterpart that is fabricated by nanolithography. We uncovered the underlying processes in the training and memory by examining the directivity and intensity as a function of time. This revealed the presence of different mechanisms, with each their own timescale. Nucleation of the iodide-rich emitter happens at a millisecond timescale, followed by further light-driven halide segregation during seconds to minutes. Competition for iodide causes further optimization over the course of tens of minutes. In the dark, the halides diffuse back within a minute, but atomic-scale changes that facilitate rapid re-segregation at the designed nucleation site remain for up to one hour. Light emission predominantly originates from the iodide-rich regions, due to energy funneling that happens at the femtosecond to picosecond time scale.^[21] The presence of these different time scales makes it possible to train the system over time and provides it with a memory for the previously trained task.

This system has the capability to process an input and optimize itself to provide an output that is an adapted copy of the input signal. Once trained for a specific input pattern (in this case study simply a plane wave), it responds by mimicking this pattern. To any other input, it will reply with a much weaker

response. Therefore, it complies with typical requirements for basic learning and memory capabilities in the social sciences,^[36,37] as well as recent characteristics identified for intelligent matter.^[38] This proof of concept also gives the prospect for more complex learning tasks, for example leveraging reciprocity to enable pattern recognition. What we present here is the discovery of a new way of looking at the dynamics in mixed halide perovskites and a case study of how this can be used to our advantage. The insight of using material instability as a feature, to reconfigure the perovskite in a desired manner, can lead to a plethora of applications for intelligent optoelectronic materials.

4. Experimental Section

Simulations: Optical simulations for the lens design were done with Finite-Difference Time-Domain simulations using the software program Lumerical. The directivity of the system was calculated using the open-source matlab code RETOP for the near-to-far-field transformation.

Sample Fabrication Chemicals: lead acetate trihydrate ($\text{Pb}(\text{CH}_3\text{COO})_2 \cdot 3\text{H}_2\text{O}$, 99.999%), dimethyl sulfoxide (DMSO, anhydrous $\geq 99.9\%$), and *N,N*-dimethylformaldehyde (DMF, anhydrous $\geq 99.8\%$) were purchased from Sigma-Aldrich. Methylammonium bromide (MABr, $\text{CH}_3\text{NH}_3\text{Br}$, 98%), Lead iodide (PbI_2 , $>98\%$), lead bromide (PbBr_2 , $>98\%$), methylammonium acetate (MAAc, $\text{CH}_3\text{NH}_3\text{CH}_3\text{COO}$, $>98\%$), and PMMA were purchased from TCI. Methylammonium iodide (MAI, $\text{CH}_3\text{NH}_3\text{I}$) was purchased from Solaronix. All chemicals were used as received.

Fabrication of thin films: Borosilicate glass substrate were thoroughly cleaned and UV-ozone surface was treated. Mixed halide perovskite films were spin coated in a nitrogen glovebox from an 0.64 M equimolar precursor solution of MAI, MABr, PbI_2 , and PbBr_2 in DMF. 150 μL was drop casted and spun for 40 seconds. At 10 s, 170 μL of chlorobenzene was dropcasted as an antisolvent. Subsequently, the samples were annealed at 100 $^\circ\text{C}$ for 5 min. MAPbBr_3 films were fabricated from a precursor solution of 0.56 M PbAc, 1.65 M MAAc, and 3.3 M MABr

in DMSO. 80 μL of precursor solution was drop casted and spun at 5000 rpm for 30 s, and annealed at 100 $^{\circ}\text{C}$ for 5 min. Encapsulation with 15 nm Al_2O_3 was done using an electron beam physical vapor deposition system (Polyteknik Flextura M508E). Encapsulation with PMMA was done using a solution of 10 g L^{-1} PMMA in chlorobenzene. This solution was spin coated at 3000 rpm for 30 s and annealed at 100 $^{\circ}\text{C}$ for 5 min. Encapsulation with AlO_x and SU-8 photoresist and lens fabrication was done as described in.^[33] A 1:5 diluted SU-8/cyclopentanone was used to obtain a layer of 250 nm to avoid laser damage to perovskite in the lithography process. The lenses are fabricated as described before,^[34] with two-photon lithography.

Characterization: Steady state absorbance spectra were measured using a LAMBDA 750 UV/Vis/NIR Spectrophotometer (Perkin Elmer). The spectrophotometer is equipped with an integrating sphere, a deuterium lamp and a tungsten lamp, and an InGaAs detector. X-ray diffraction patterns were recorded using a Bruker D2 phaser, using a Cu $K\alpha$ tube. Photoluminescence spectra were recorded with a confocal imaging microscope (WITec alpha300 SR) equipped with a 405 nm diode laser (Thorlabs S1FC405).

Supporting Information

Supporting Information is available from the Wiley Online Library or from the author.

Acknowledgements

This work is part of the research program Mat4Sus, which is financed by the Netherlands Organisation for Scientific Research (NWO). The work has been carried out at Amolf, an NWO funded institute. The authors thank Bas Overvelde and Martin van Hecke for their input and view on the concept of material learning, and Marc Serra Garcia for constructive criticism of the manuscript.

Conflict of Interest

The authors declare no conflict of interest.

Data Availability Statement

The data that support the findings of this study are available from the corresponding author upon reasonable request.

Keywords

directivity, material learning, perovskite, phase segregation, self-optimizing

Received: May 5, 2022

Revised: June 23, 2022

Published online:

- [1] Q. A. Akkerman, L. Manna, *ACS Energy Lett.* **2020**, *5*, 604.
 [2] L. Protesescu, S. Yakunin, M. I. Bodnarchuk, F. Krieg, R. Caputo, C. H. Hendon, R. X. Yang, A. Walsh, M. V. Kovalenko, *Nano Lett.* **2015**, *15*, 3692.
 [3] M. A. Green, A. Ho-Baillie, H. J. Snaith, *Nat. Photonics* **2014**, *8*, 506.

- [4] Z. Li, T. R. Klein, D. H. Kim, M. Yang, J. J. Berry, M. F. Van Hest, K. Zhu, *Nat. Rev. Mater.* **2018**, *3*, 18017.
 [5] W. Nie, H. Tsai, R. Asadpour, J. C. Blancon, A. J. Neukirch, G. Gupta, J. J. Crochet, M. Chhowalla, S. Tretiak, M. A. Alam, H. L. Wang, A. D. Mohite, *Science* **2015**, *347*, 522.
 [6] W. Nie, J. C. Blancon, A. J. Neukirch, K. Appavoo, H. Tsai, M. Chhowalla, M. A. Alam, M. Y. Sfeir, C. Katan, J. Even, S. Tretiak, J. J. Crochet, G. Gupta, A. D. Mohite, *Nat. Commun.* **2016**, *7*, 11574.
 [7] E. Bi, Z. Song, C. Li, Z. Wu, Y. Yan, *Trends in Chemistry* **2021**, *3*, 575.
 [8] S. S. Mali, J. V. Patil, H. Arandiyani, R. Luque, C. K. Hong, *ECSJ. Solid State Sci. Technol.* **2019**, *8*, Q111.
 [9] J. A. Christians, S. N. Habisreutinger, J. J. Berry, J. M. Luther, *ACS Energy Lett.* **2018**, *3*, 2136.
 [10] A. J. Knight, A. D. Wright, J. B. Patel, D. P. McMeekin, H. J. Snaith, M. B. Johnston, L. M. Herz, *ACS Energy Lett.* **2019**, *4*, 75.
 [11] Y. Zhong, C. A. M. Luna, R. Hildner, C. Li, S. Huettnner, *APL Mater.* **2019**, *7*, 041114.
 [12] A. J. Barker, A. Sadhanala, F. Deschler, M. Gandini, S. P. Senanayak, P. M. Pearce, E. Mosconi, A. J. Pearson, Y. Wu, A. R. Srimath Kandada, T. Leijtens, F. De Angelis, S. E. Dutton, A. Petrozza, R. H. Friend, *ACS Energy Lett.* **2017**, *2*, 1416.
 [13] E. T. Hoke, D. J. Slotcavage, E. R. Dohner, A. R. Bowring, H. I. Karunadasa, M. D. McGehee, *Chem. Sci.* **2015**, *6*, 613.
 [14] S. Mahesh, J. M. Ball, R. D. Oliver, D. P. McMeekin, P. K. Nayak, M. B. Johnston, H. J. Snaith, *Energy and Environmental Science* **2020**, *13*, 258.
 [15] A. Walther, *Adv. Mater.* **2020**, *32*, 20.
 [16] R. Merindol, A. Walther, *Chem. Soc. Rev.* **2017**, *46*, 5588.
 [17] Z. Wang, J. Wang, J. Ayarza, T. Steeves, Z. Hu, S. Manna, A. P. Esser-Kahn, *Nat. Mater.* **2021**, *20*, 869.
 [18] W. Zhang, B. Gao, J. Tang, P. Yao, S. Yu, M. F. Chang, H. J. Yoo, H. Qian, H. Wu, *Nat. Electron.* **2020**, *3*, 371.
 [19] J. Feldmann, N. Youngblood, C. D. Wright, H. Bhaskaran, W. H. Pernice, *Nature* **2019**, *569*, 208.
 [20] M. L. De Giorgi, S. Milanese, A. Klini, M. Anni, *Molecules* **2021**, *26*, 3.
 [21] M. Yuan, L. N. Quan, R. Comin, G. Walters, R. Sabatini, O. Voznyy, S. Hoogland, Y. Zhao, E. M. Beauregard, P. Kanjanaboos, Z. Lu, D. H. Kim, E. H. Sargent, *Nat. Nanotechnol.* **2016**, *11*, 872.
 [22] S. J. Yoon, S. Draguta, J. S. Manser, O. Sharia, W. F. Schneider, M. Kuno, P. V. Kamat, *ACS Energy Lett.* **2016**, *1*, 290.
 [23] A. J. Knight, L. M. Herz, *Energy and Environmental Science* **2020**, *13*, 2024.
 [24] W. Mao, C. R. Hall, S. Bernardi, Y. B. Cheng, A. Widmer-Cooper, T. A. Smith, U. Bach, *Nat. Mater.* **2021**, *20*, 55.
 [25] D. T. Limmer, N. S. Ginsberg, *J. Chem. Phys.* **2020**, *152*, 230901.
 [26] Y. Wang, X. Quintana, J. Kim, X. Guan, L. Hu, C.-H. Lin, B. T. Jones, W. Chen, X. Wen, H. Gao, T. Wu, *Photonics Research* **2020**, *8*, A56.
 [27] J. S. Yun, J. Seidel, J. Kim, A. M. Soufiani, S. Huang, J. Lau, N. J. Jeon, S. I. Seok, M. A. Green, A. Ho-Baillie, *Adv. Energy Mater.* **2016**, *6*, 1.
 [28] D. J. Slotcavage, H. I. Karunadasa, M. D. McGehee, *ACS Energy Lett.* **2016**, *1*, 1199.
 [29] W. Mao, C. R. Hall, A. S. Chesman, C. Forsyth, Y. B. Cheng, N. W. Duffy, T. A. Smith, U. Bach, *Angewandte Chemie - International Edition* **2019**, *58*, 2893.
 [30] H. H. Fang, S. Adjokatse, H. Wei, J. Yang, G. R. Blake, J. Huang, J. Even, M. A. Loi, *Sci. Adv.* **2016**, *2*, 1.
 [31] T. Hirvikorpi, M. Vähä-Nissi, T. Mustonen, E. Iiskola, M. Karppinen, *Thin Solid Films* **2010**, *518*, 2654.
 [32] D. Raffaele Ceratti, Y. Rakita, L. Cremonesi, R. Tenne, V. Kalchenko, M. Elbaum, D. Oron, M. Alberto Carlo Potenza, G. Hodes, D. Cahen, *Adv. Mater.* **2018**, *30*, 1706273.

- [33] J. S. Van Der Burgt, C. D. Dieleman, E. Johlin, J. J. Geuchies, A. J. Houtepen, B. Ehrler, E. C. Garnett, *ACS Photonics* **2021**, *8*, 1143.
- [34] E. Johlin, S. A. Mann, S. Kasture, A. F. Koenderink, E. C. Garnett, *Nat. Commun.* **2018**, *9*, 4742.
- [35] L. Novotny, B. Hecht, *Principles of nano-optics*, Cambridge University Press, Cambridge **2009**.
- [36] S. J. Lachman, *Journal of Psychology: Interdisciplinary and Applied* **1997**, *131*, 477.
- [37] J. de Houwer, D. Barnes-Holmes, A. Moors, *Psychonomic Bulletin and Review* **2013**, *20*, 631.
- [38] C. Kaspar, B. J. Ravoo, W. G. van der Wiel, S. V. Wegner, W. H. Pernice, *Nature* **2021**, *594*, 345.